Impact of co-injected impurities on hydrodynamics of CO2 injection. Studying interplayed chromatographic partitioning and density driven flow and fate of the injected mixed gases: numerical and experimental results.

Irina Sin, Jérôme Corvisier

14th International Conference on Greenhouse Gas Control Technologies, GHGT-14

21st -25th October 2018, Melbourne, Australia

Impact of co-injected impurities on hydrodynamics of CO_2 injection. Studying interplayed chromatographic partitioning and density driven flow and fate of the injected mixed gases: numerical and experimental results.

Irina Sin[a,]*, Jérôme Corvisier[a]

[a]*MINES ParisTech, PSL University, Centre de Géosciences, 35 rue Saint-Honoré 77305 Fontainebleau, France*

Abstract

This work presented a study on the chromatographic partitioning of CO_2 and impurities present in the injected stream in the CCS context. Laboratory and field observations have already revealed the chromatographic partitioning phenomenon of CO_2 and impurities both in the gas and in the aqueous phases. Series of laboratory experiments are modeled using the reactive transport HYTEC. Numerical results confirm the laboratory observations and show differential breakthrough of injected gases. A series of experiments on CO_2 and H_2S mixture with different H_2S concentration is modeled. Numerical results of HYTEC are successfully compared with the results given by CMG-GEM and with experimental data. Another series of dynamic displacement-solubility experiments is modeled to study the chromatographic gas partitioning depending on a type of impurity such as H_2S, CH_4, N_2, SO_2. O_2, and Ar. Numerical results show that the physics can be modeled both qualitatively and quantitatively. 1. Solubility of the impurity in the injected stream regarding to that of CO_2 is a key factor. The less soluble the impurity gas is, the earlier and higher breakthrough should be expected. 2. Classification of impurity gases can be proposed. For example, in the decreasing order of their solubility (13.5 MPa, 61°C, 118950 ppm): $SO_2 > H_2S > CO_2 > CH_4 > Ar > O_2 > N_2$. 3. Using accurate models of reactive transport, solubility, phase equilibrium and thermodynamic properties of non-ideal mixtures allows reproducing of the chromatographic partitioning: breakthrough time of gases, gas concentration, and front propagation. Chromatographic partitioning was studied at reservoir scale by modeling two scenarios of impure CO_2 injection over 30 years: $95\%CO_2+4\%N_2+1\%O_2$ and $95\%CO_2+5\%SO_2$. When injecting impurities, the chromatographic partitioning can be observed inside the gas plume and in the aqueous solution. Modeling injection of $95\%CO_2+4\%N_2+1\%O_2$ demonstrated potential usage of noble gases for monitoring and proved the previous laboratory results. The plume composition strongly depends on a type of the co-injected gas. Moreover, a type of impurity and its concentration change the density of gas current and the density of the formation water with dissolved components. Both densities in the case of $95\%CO_2+5\%SO_2$ injection are overall higher than those in the $95\%CO_2+4\%N_2+1\%O_2$ model. This impacts on the buoyancy forces, hence on the distance, velocity and shape of the plume. Since dissolved impurities contribute to the liquid density, it can then accelerate or slow convective dissolution. Heterogeneous gas composition induces density driven motion that can be especially important in case of heavy compounds such as SO_2.

Keywords: CO_2 storage; impurities; chromatographic partitioning; density-driven flow; numerical modeling; CO_2; N_2; O_2; SO_2; Ar; H_2S; CH_4.

* Corresponding author. Tel.: +331-6469-4812.
E-mail address: irina.sin@mines-paristech.fr

1. Introduction

During the capture process, CO_2 should be separated to increase the efficiency of the storage and to respect the environmental and legal aspects. The injection stream can still contain small amounts of impurities such as N_2, O_2, Ar, CO, SO_x, NO_x, CH_4, H_2S and H_2 [1, 2]. Composition and concentration of co-contaminant gas vary depending on major CO_2 source, type of industry and capture process. Some of them can negatively affect the integrity of geological site and/or pipelines or reduce the CO_2 storage capacity. Purifying injection stream involves additional power demand. Understanding their impact on CCS is essential to define the allowed maximum concentration of co-contaminant and to optimize the overall cost.

Small amount of impurities of 5% may still remain after gas separation process. Investigation of their impact has been started over the last two decades: studies on a type of impurity, its concentration [3] and thermodynamic properties, consequences on storage capacity [4,5], experimental and numerical models on geochemical reactions [6,7,8,9], modeling injection of impure CO_2 at large-scale [10-14], field observations of gas migration [15].

Previous works on experimentally and numerically thermodynamic properties of several CO_2 binary mixtures [4-9,16] highlighted the positive density and solubility effects of SO_2 and the negative impact of CH_4, Ar, O_2 and N_2 on the volume and solubility storage capacity. However, comparing to low reactive gases as nitrogen, argon or methane such impurities as SO_2 and H_2S are highly chemically reactive. They can cause an alteration of reservoir and caprock minerals and near wellbore area in particular. For example, even a very small concentration of SO_2 leads to a strong acidification of the brine. Once sulfur dioxide dissolves and pH drops, it then can induce the dissolution of carbonates such as calcite and the precipitation of sulfate minerals such as anhydrite. This was experimentally and numerically demonstrated in [8].

Beside the pure geochemical effects, other physical phenomena have been observed in the presence of impurities. Several field and laboratory observations showed differential breakthrough of injected gases [3,15].

- When a mixture of 98% CO_2 and 2% H_2S was injected, an earlier breakthrough of CO_2 prior to H_2S was detected at producing wells.
- When a CO_2-rich mixture with N_2 and O_2 was injected, earlier arrivals both of dissolved oxygen and of oxygen-nitrogen gas mixture were observed.

Chromatographic gas partitioning depending on a type of impurity was studied in [3]. Behavior of CO_2 binary systems with H_2S, CH_4, N_2, and SO_2 was demonstrated during flow experiments. Laboratory results revealed a key factor of the impurity solubility order regarding to that of CO2.

In this work, these dynamic displacement-solubility experiments have been modeled. Numerical simulations for N_2, SO_2, CH_4, and H_2S have been performed. The role of differential solubility in chromatographic gas partitioning has been confirmed and the concept has been complemented with O_2, Ar.

Moreover, the type and concentration of impurities changes gas and liquid densities. This changes the buoyancy forces, hence the distance, velocity and shape of the plume spread. This work presents multiphase multicomponent reactive flow and transport simulations of injection of impure CO2 at reservoir-scale. Dissolved impurities contribute to liquid density and can then accelerate or slow convective dissolution. Heterogeneous gas composition induces density driven motion that can be especially important in case of heavy compounds. When injecting impurities, chromatographic partitioning can be observed inside the gas plume. Plume composition depends on type of co-injected gas.

The numerical simulations presented in this work were performed using the reactive transport code HYTEC [17-19] and its geochemical core CHESS [8,9,20,21]. Last developments on gas-water-rock interactions allow complex modeling of real gas behavior, solubility in single and mixed brines, thermodynamic properties and coupled multiphase multicomponent flow and reactive transport.

Section 2 briefly describes the mathematical and numerical methods used to perform the multiphase multicomponent reactive flow and transport simulations. Section 3 shows the model of flow experiment and numerical results of chromatographic gas partitioning. Section 4 presents two models of impure CO2 injection at reservoir scale whose numerical results give insights of gas current motion, its heterogeneous composition and density driven dynamics. We make the conclusions in Section 5.

2. Mathematical and numerical methods

HYTEC is a reactive transport simulator [17-19], which was widely evaluated in benchmark studies [22-24] and applied in various applications such as cement degradation [25] radioactive waste disposal [26], geological storage of acid gases [8,27,28] and uranium in situ recovery processes [29]. The code is based on a finite-volume method and deals both with structured and with unstructured grids. Its geochemical part CHESS allows modeling interface reactions, precipitation, dissolution, organic compounds, redox reactions and isotopic fractionation. Both reactions at equilibrium and kinetics can be modeled. Morel's method is used to formulate the chemical system, which is then solved by a modified Newton's method. The activity coefficients γ_i of non-ideal aqueous solutions can be calculated by applying different activity models such as the specific ion theory (SIT) [31]. The fugacity-activity ($\varphi - \gamma$) approach is used to solve the gas-liquid equilibrium (1):

$$P y_i \varphi_i^g = K_i^h \gamma_i x_i, \tag{1}$$

where P is the pressure, y_i is the gas mole fraction of species i, K_i^h is the corrected Henry's constant of species i, x_i is the mole fraction of species i in the liquid phase. $K_i^h = K_i^h(T,P)$ comprises the Poynting factor and corrects the reference fugacity with respect to the pressure and the temperature:

$$K_i^h(T,P) = K_i^h(T,P^{sat})\exp\left(\frac{v_i^\infty (P-P^{sat})}{RT}\right) \tag{2}$$

where P^{sat} is the saturation vapor pressure, v_i^∞ is the molar volume of species i at infinite dilution. The fugacity coefficients are calculated using an equation of states (EOS). CHESS/HYTEC proposes a wide range of EOS. We chose the Peng-Robinson EOS (PR78) [32]:

$$P = \frac{RT}{v-b_i} - \frac{a_i(T)}{v(v+b_i)+b_i(v-b_i)} \tag{3}$$

where the repulsive and attractive terms are functions of the critical pressure $P_{c,i}$, critical temperature $T_{c,i}$ and the acentric factor ω_i (see details in [32]). For mixtures, the parameters a and b are calculated via the combining rule for the cross parameter a_{ij} and the quadratic mixing rules for a and b:

$$a = \sum_i \sum_j x_i x_j a_{ij} \tag{4}$$

$$a_{ij} = \sqrt{a_i a_j}(1 - k_{ij}) \tag{5}$$

$$b = \sum_i x_i b_i \tag{6}$$

where k_{ij} are the binary interaction parameters. In [33], the predictive PR78 (PPR78) was proposed where the binary interaction parameters can be calculated and depend on the temperature. In [34], a volume translated method (VTPR) was proposed to improve modeling of volumetric properties. The pseudo partial molar volume is then introduced:

$$\tilde{v}_i = v_i + c_i \tag{7}$$

where c_i is the constant translation parameter or the correction of molar volume. Calculation methods of c_i can be found in [34].

Table 1. Binary interaction parameters k_{ij} and partial molar volume at infinite dilution v_i^{∞}.

Compound	k_{i,H_2O}	k_{i,CO_2}	v_i^{∞}, cm^3/mol
CO_2	0.199		28.10
N_2	0.428	-0.007	34.53
O_2	0.606	0.114	39.70
Ar	0.569	0.163	32.92
CH_4	0.506	0.090	36.20
H_2S	0.143	0.097	38.15
SO_2	0.100	0.046	39.76

The approach was applied to model solubility of gas components and binary systems in pure water, salt and complex brine solutions [8,9,27]. The authors have compared numerical results of the proposed EOS-based method, GC-PR-CPA for Cubic Plus Association using Peng-Robinson EOS and the Group Contribution method [30] and experimental data. New numerical results on modeling gas mixture-water-rock experiments are presented in [21]. Moreover, the approach has been extended to model the volumetric properties of pure compounds and binary mixtures using the PPR78 and VTPR [13]. Numerical results have been compared with other EOS (PR78, PPR78, T-VTPR, CPA models and GERG-2008 (REFPROP)), experimental and NIST data in [13]. The approach can be applied to ternary or multicomponent systems, even though their accuracy may be questioned due to lack of required datasets. Nevertheless, the method allows for a detailed investigation of highly coupled hydrodynamic and chemical processes involved in the impure CO2 injection problems at different scales.

HYTEC is based on the operator-splitting approach that integrates not only all functionalities of CHESS but also numerous thermo-hydrodynamic modules (e.g., saturated, unsaturated, two-phase flow, heat and isothermal regimes). A special sequential iterative coupling method [19] is applied for modelling compressible two-phase flow and reactive transport. This method ensures flexibility of each module, allows sophisticated modelling of hydrodynamics, thermodynamics and geochemistry. The coupling method was verified on benchmark problems and compared with TOUGH2-ECO2, TOUGH2 (CSIRO), DUNE, GEM and STOMP [19].

The presented methods have been used for the numerical models in this work.

3. Chromatographic partitioning

Chromatographic partitioning of injected gas was investigated experimentally in [3], in which the authors provided the sensitivity study on the impact of gas impurity concentration (2, 5, 30% of H_2S), on the impact of pressure, temperature and salinity conditions (61°C and 13.5 MPa; 25°C and 6 MPa; fresh water and 119 ppm of salinity) and of admixture type in the injected stream (H_2S, N_2, SO_2, CH_4). In the last stage, the laboratory results revealed a key factor of the impurity solubility order regarding to that of CO_2. The breakthrough time of the gas compounds and their profiles highly depend on the solubility ratio between gases. The less soluble the admixture gas is, the earlier and higher breakthrough is expected. The impurity gases present in the injection stream after the capture processes can then be classified by the solubility.

A series of experiments with variable H_2S concentration in the injected gas stream was chosen for modeling. Numerical simulations were performed by CMG-GEM™ and presented in [35]. The laboratory experiments have been modeled by HYTEC. The present section shows our numerical results comparing with the experimental and numerical results obtained in [3,35]. The dynamic displacement solubility experiments selected for modeling are shortly described in Section 3.1 as well as the model description. Section 3.2 demonstrates the flow evolution and physics of the H_2S experiments. Section 3.3 shows the extending the numerical model to other types of admixture and confirms the used methods (Section 2) and the laboratory results on chromatographic gas partitioning.

3.1. Numerical model of laboratory experiments

The dynamic solubility experiments were carried out at high pressure and temperature conditions in a tube homogeneously packed with silicate rounded frac sand. The length of the tube is 24.38 m; the tube inner diameter is 0.775 cm. The porosity and permeability are 0.37 and 5915 mD, respectively. The gas mixture is injected at a constant rate of 7.5 cm^3/h in the tube at constant pressure 13.5 MPa, temperature 61°C and brine salinity 118950 ppm. Modeling of viscosities and densities may be different from [35]. The gas and brine viscosities are constant in this study 0.037 and 0.579 mPa·s, respectively. The gas density is modeled according the PR78, which is reliable for the gas mixtures. The McCain model [36] was chosen for the brine density. Fitting of relative permeability functions for gas and brine is reported in details in [3]. Curves were fitted only for H_2S and CO_2 experiments.

The methods of gas-liquid equilibrium are described in Section 2. The binary interaction parameters k_{ij} and the partial molar volume at infinite dilution v_i^{∞} used in this study are given in Table 1. In this study, the partial molar volume was globally averaged or locally averaged for several compounds (e.g., Ar, N_2, CO2, O_2, SO_2). The binary interaction parameters can be found in literature and can be calculated by the PPR78.

3.2. Numerical results of H_2S and CO_2 partitioning

Fig. 1 presents the numerical results for a feed gas of 2% H_2S and 98% CO_2. Numerical results are in a good agreement with the laboratory experiments and numerical models reported in [35]. The gas mixture is injected in the saturated tube; the gas front propagates continuously towards the outlet of the tube, Fig. 1a. The numerical results of CMG-GEM and HYTEC are similar. The gas saturation curves have a common shape and evolution. Fig. 2 shows the evolution of gas composition at the outlet of the tube for the cases of 2% H_2S and 30% H_2S in the injected stream. The breakthrough of H_2S is delayed in both cases. Only slight differences between experimental and numerical results can be observed. However, the numerical models give a phenomenological description of the experiment.

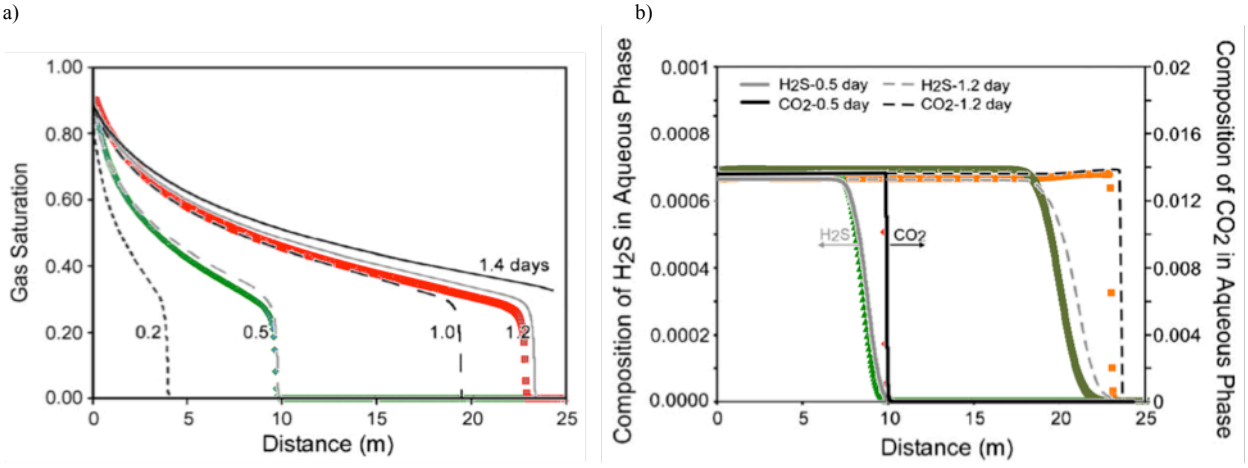

Fig. 1. Numerical results of the laboratory experiment [3,35] modeled by CMG-GEM (black lines) and HYTEC (colored lines). Injection of a feed gas of 2% H_2S and 98% CO_2 in a long sand-packed coil. a) Gas saturation evolution. b) Composition in mole fraction of H_2S and CO_2 in the aqueous phase at 0.5 and 1.2 days.

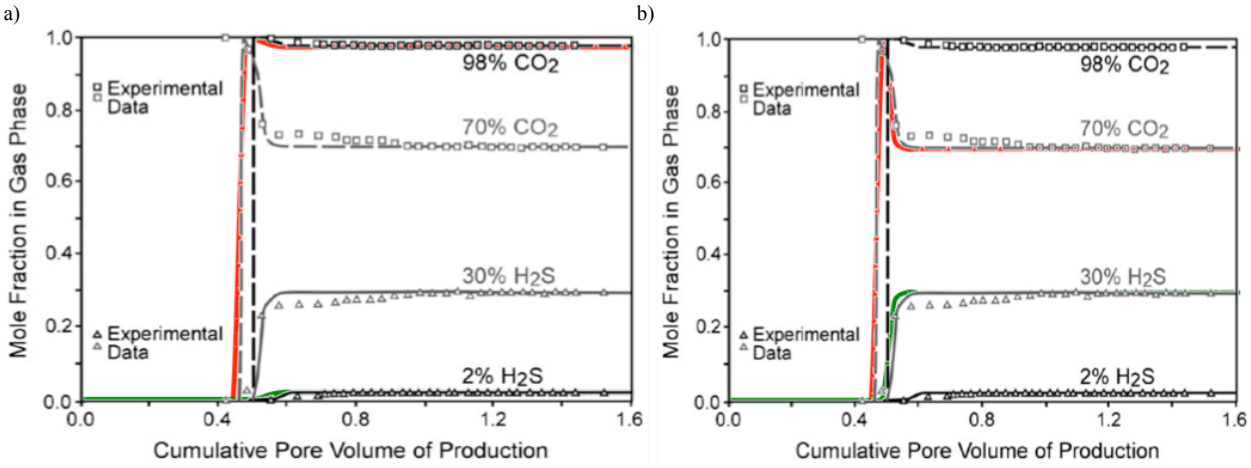

Fig. 2. Numerical results of the laboratory experiment [3,35] modeled by CMG-GEM (black lines) and HYTEC (colored lines) compared with experimental data (symbols). Composition in mole fraction of H_2S and CO_2 in the gas phase during injection of a) 2% H_2S and 98% CO_2 and b) 30% H_2S and 70% CO_2 gas mixture in a long sand-packed coil.

Since H_2S is more soluble than CO_2, the breakthrough gas is CO_2-rich. The H_2S breakthrough indeed occurs later but it then rises and reaches its concentration in the feed gas. The composition of CO_2 and H_2S in the aqueous phase at 0.5 and 1.2 days is shown in Fig. 1b. Retardation of H_2S front can be observed and its gap with the CO_2 front grows with injection time. This dynamics is explained by a higher solubility of H_2S with regard to CO_2. The partitioning of H_2S and CO_2 both in the gas phase and aqueous solution is observed. The numerical models qualitatively reproduce the laboratory experiment.

3.3. Numerical results for SO_2, H_2S, CH_4, Ar, O_2, and N_2 cases

For the same flow conditions, the authors of [3] performed a series of experiments with different impurities in the feed gas. The experiments were done with 5% of H_2S, N_2, SO_2 and CH_4 in the injected stream. The breakthrough of gases was monitored. The experiments show a key role of differential solubility of gases in the feed gas. In Fig. 3, the mole fraction of the impurity gas H_2S, N_2, SO_2 and C1 (methane) are normalized by the relevant initial mole fraction of the injected gas (5% for all four tests) in order to emphasize the scale of the gas partitioning effect due to the different solubility relations. We compare the experimental data and numerical results of HYTEC in Fig. 3a. Despite a small mismatch the numerical model confirms the experimental data. Since the curves of relative permeability were fitted only for H_2S and CO_2 experiments, that may explain difference between numerical and experimental results. These results confirm that

- The solubility of the impurity in the injected stream regarding to that of CO_2 is a key factor. The less soluble the impurity gas is, the earlier and higher breakthrough should be expected.

- Classification of impurity gases can be proposed. For example, in the decreasing order of their solubility (13.5 MPa, 61°C, 118950 ppm): $SO_2 > H_2S > CO_2 > CH_4 > Ar > O_2 > N_2$.

Hence, the gases on the RHS to CO2 of the inequality (from CH_4 to N_2) should evolve the similar profile of the normalized mole fraction with high and early peaks at the edge front of the breakthrough gas, and vice versa, SO_2 and H_2S yield a lower and later breakthrough. To complete the sequence of experiments, we performed the simulations with 5% Ar and 5% O2 in the 95% CO_2 feed gas. Fg. 3b brings together the six cases of the 5% impurity gas in the injected stream.

a)

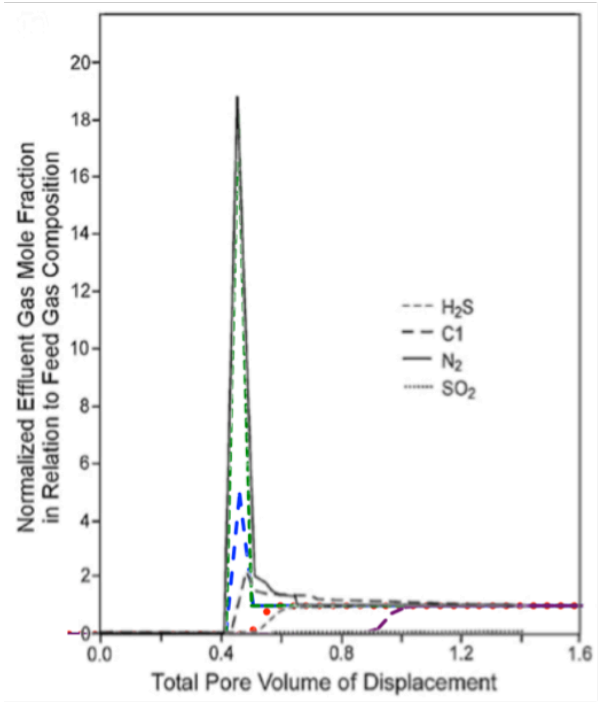

b)

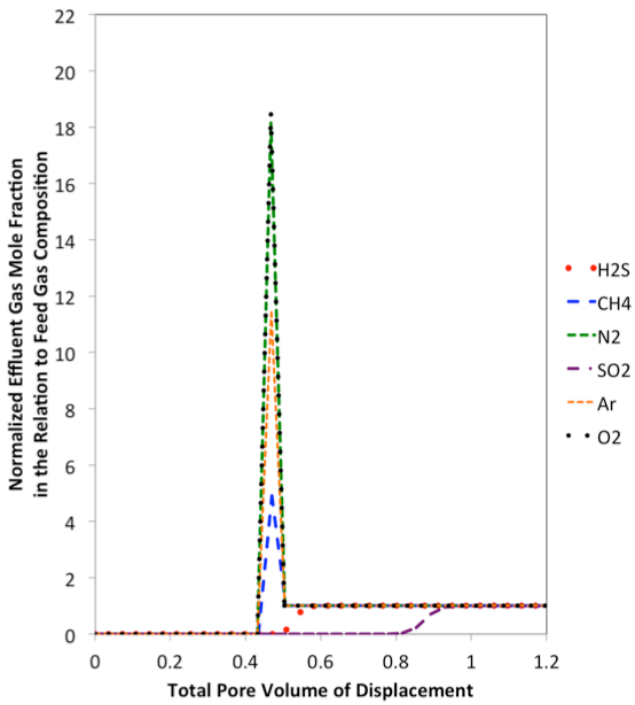

Fig. 3. a) Mole fraction of the impurity gases, H_2S, N_2, SO_2, C1 (CH_4) at the outlet, normalized by the relevant mole fraction in the initially injected gas (5% for all cases), as a function of the pore volume of the total injection. Comparison of experimental data [3] (black lines) and numerical results of HYTEC (colored lines). b) Mole fraction of the impurity gases at the outlet for H_2S, N_2, SO_2, C1 (CH_4) complemented by Ar and O_2. Numerical results only.

4. Injection of impure CO_2 and convective mixing

4.1. Problem description

Modeling of CO_2 injection at reservoir scale allows for analysis of the gas plume evolution and undergoing processes. Supercritical CO_2 is injected through a well in a vertically confined long aquifer with a height of 100 m at a depth of 1100 m, see Fig. 4. The injection rate is constant, 10 kg/s; the well radius is 0.3 m; the injection is performed over the whole area of the well during 30 y. Supposing a homogeneous medium, the 2D axisymmetric problem is set: 0.2 of porosity, 10^{-12} m^2 of permeability. The Brooks-Corey models [37] are chosen to model the capillary pressure and relative permeability with $p_b = 10^5$ Pa, $\lambda = 2$, $S_{lr} = 0.15$, $S_{gr} = 0.05$. The gas and liquid densities are modeled by the PR78 and the T-VTPR, respectively. The gas and liquid viscosities are considered constant: 2.84×10^{-5} and 5.49×10^{-5} Pa·s, respectively. The gas and liquid diffusion coefficients are also constant: 1.95×10^{-7} and 3.36×10^{-9} m2/s, respectively. The length of the aquifer is 10 km. Length of cells varies from 2 to 1000 m that allows us to reduce the grid dimension to 33,250 cells.

Considering the observations on chromatographic partitioning given in Section 3, we devise two feed gas scenarios:

- 95% CO_2, 4% N_2 and 1% O_2 and
- 95% CO_2 and 5% SO_2.

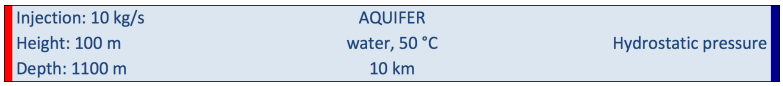

Fig. 4. Schematic of 2D radial problem.

Though $H_2O_{(g)}$ can be neglected, it has been added in the chemical system of the problem. Since N_2 and O_2 are less soluble that CO_2, they can be expected at the edge of the gas current. The gas mixture with these impurities becomes lighter, the density of current drops. This may promote the plume spreading. An opposite effect leads adding SO_2 in the feed gas. Being more soluble that CO_2, SO_2 spreading should be delayed comparing to CO_2 propagation. The presence of SO_2 makes both the gas current and the formation water with dissolved species heavier. Therefore, a higher convective mixing can be expected that causes CO_2 dissolution.

4.2. Numerical results

Fig. 5 shows a gas front evolution and its composition in mole fraction after 30 y of the CO_2+N_2+O_2 injection. Gas current has a conventional plume shape, Fig. 5a. Partitioning of CO_2, N_2 and O_2 is visible: N_2 and O_2 form a noticeable front at the plume edge, Fig. 5b, c and d. This favorable aspect makes them interesting for monitoring usage. $H_2O_{(g)}$ can indeed be eliminated from the chemical system, Fig. 5d. Partitioning in the liquid phase is also apparent, Fig. 6. The density of the aqueous solution that contains dissolved species (CO_2, N_2 and O_2 in this case) is higher than the density of the formation water. This evolves instabilities, which initiate under the plume, create convective motion and moreover, enhances dissolution of gas species. Fig. 6 demonstrates CO_2, N_2 and O_2 rich fingering. An accurate modeling of non-ideal gaseous mixtures and aqueous solution and their thermodynamic properties is required to replicate an adequate plume propagation, its composition, and a representative rate of convective fluxes.

When injecting CO_2+SO_2, there is an opposite gas partitioning, Fig. 7. SO_2 motion is delayed because of its higher solubility. CO_2 spreads further than SO_2 in the aqueous phase as well, Fig. 8. Near-well fingers are of a higher SO_2 concentration. SO_2 has a potentially favorable property: SO_2 mixtures have higher density. Its impact both on the gas density and on the liquid density is significant. The effect can be seen in Figs. 9 and 10, where the gas and liquid densities are mapped for both scenarios. The gas current of the CO_2+SO_2 case is much heavier, especially near the injection well area. Convective mixing is also more pronounced in the CO_2+SO_2 case, that evolves a higher dissolution rate. A more detailed analysis of convective fluxes is still needed to evaluate it quantitatively. Also, SO_2 can cause a corrosion of well materials and a strong acidification of the formation water.

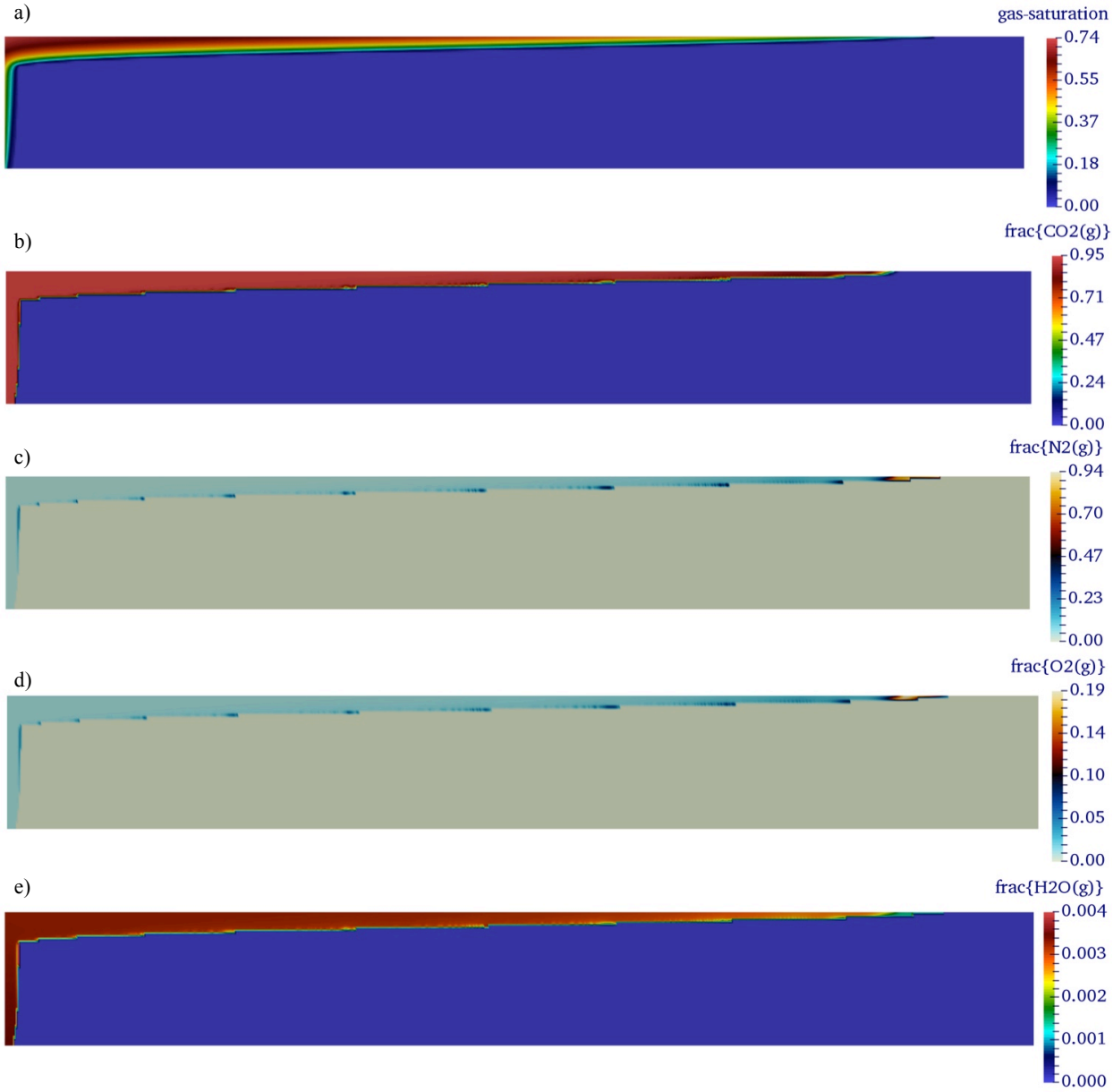

Fig. 5. Injection of 95% CO_2, 4% N_2, and 1% O_2. a) Gas saturation map and gas composition in mole fraction of b) $CO_{2(g)}$, c) $N_{2(g)}$, d) $O_{2(g)}$, and e) $H_2O_{(g)}$ after 30 y of injection. Rescaled zone of reservoir [3000 x 100] m.

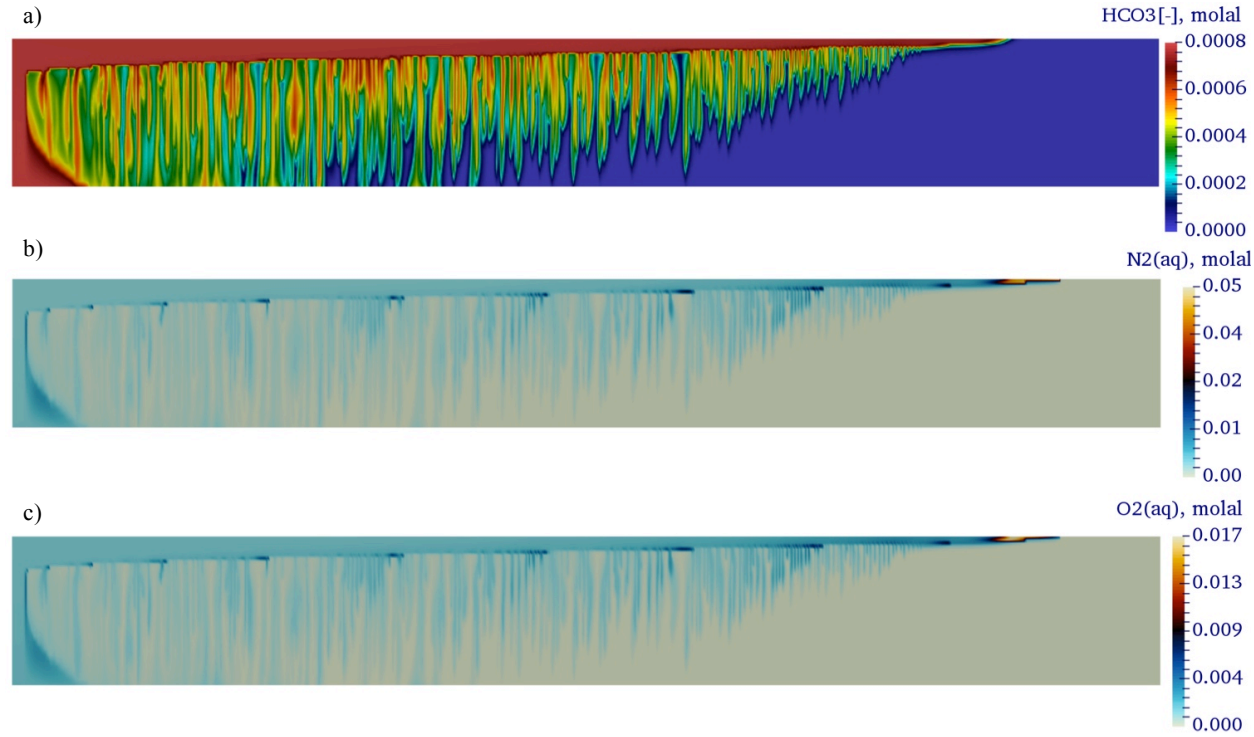

Fig. 6. Injection of 95% CO_2, 4% N_2, and 1% O_2. Aqueous composition in molal: a) HCO_3^-, b) $N_{2(aq)}$, and c) $O_{2(aq)}$ after 30 y of injection. Rescaled zone of reservoir [3000 x 100] m.

Fig. 7. Injection of 95% CO_2 and 5% SO_2. Gas composition in mole fraction: a) $CO_{2(g)}$ and b) $SO_{2(g)}$ after 30 y of injection. Rescaled zone of reservoir [3000 x 100] m.

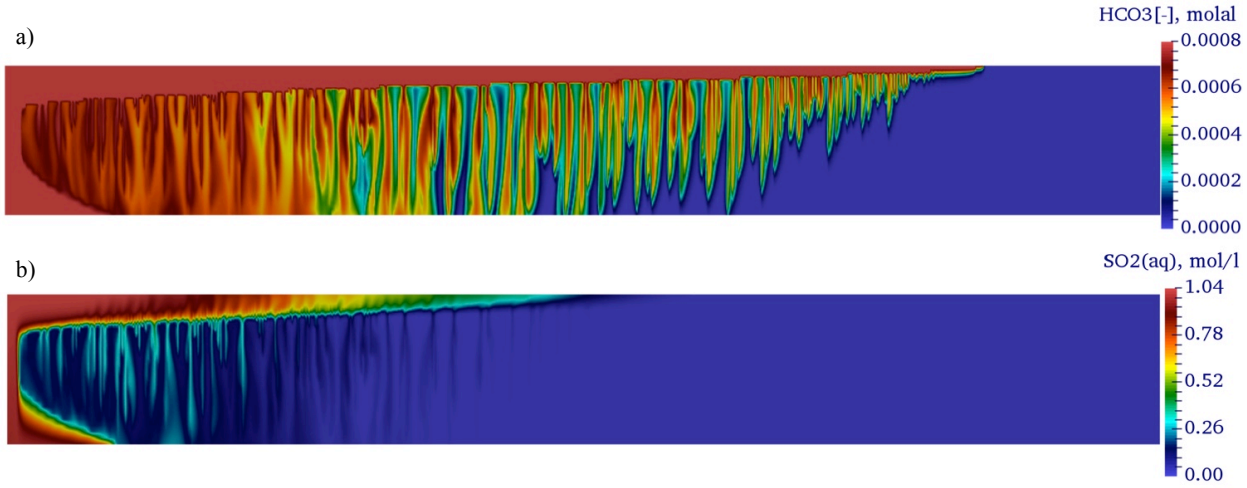

Fig. 8. Injection of 95% CO_2 and 5% SO_2. Aqueous composition: a) $CO_{2(aq)}$ in molal and b) $SO_{2(aq)}$ in mol/l after 30 y of injection. Rescaled zone of reservoir [3000 x 100] m.

Fig. 9. Gas density map after 30 injection of a) 95% CO_2, 4% N_2 and 1% O_2 and of b) 95% CO_2 and 5% SO_2 feed gas. Rescaled zone of reservoir [3000 x 100] m.

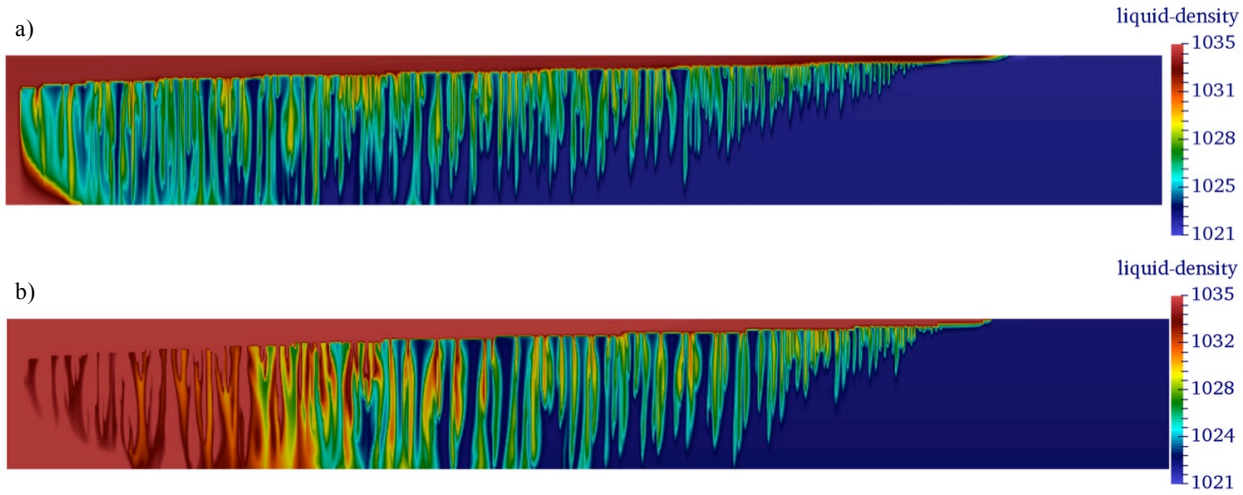

Fig. 10. Liquid density map after 30 injection of a) 95% CO_2, 4% N_2 and 1% O_2 and of b) 95% CO_2 and 5% SO_2 feed gas. Rescaled zone of reservoir [3000 x 100] m.

5. Conclusions

This work presented a study on the chromatographic partitioning of CO_2 and impurities present in the injected stream in the CCS context. Laboratory and field observations have revealed the chromatographic partitioning phenomenon of CO_2 and impurities both in the gas and in the aqueous phases [3,15,38]. Series of laboratory experiments were modeled using the reactive transport HYTEC. Numerical results confirmed the laboratory observations and showed differential breakthrough of injected gases.

A series of experiments on CO_2 and H_2S mixture with different H_2S concentration was modeled. Numerical results of HYTEC are in good agreement both with the results given by CMG-GEM and with experimental data.

Another series of dynamic displacement-solubility experiments was modeled to study the chromatographic gas partitioning depending on a type of impurity. Numerical results show that the physics can be modeled both qualitatively and quantitatively. The experiments were carried out for several impurities: H_2S, CH_4, N_2, and SO_2. Considering the same flow conditions, numerical models for O_2, Ar were additionally constructed. Next conclusions can be made:

- Solubility of the impurity in the injected stream regarding to that of CO_2 is a key factor. The less soluble the impurity gas is, the earlier and higher breakthrough should be expected.

- Classification of impurity gases can be proposed, in the decreasing order of their solubility (13.5 MPa, 61°C, 118950 ppm): SO_2 > H_2S > CO_2 > CH_4 > Ar > O_2 > N_2. Hence, the gases on the RHS to CO2 of the inequality (from CH_4 to N_2) should evolve the similar profile of the normalized mole fraction with high and early peaks at the edge front of the breakthrough gas, and vice versa, SO_2 and H_2S yield a lower and later breakthrough.

- Using accurate models of reactive transport, solubility, phase equilibrium and thermodynamic properties of non-ideal mixtures allows reproducing of the chromatographic partitioning: breakthrough time of gases, gas concentration, and front propagation.

Chromatographic partitioning was studied at reservoir scale by modeling two scenarios of impure CO_2 injection over 30 years: 95%CO_2+4%N_2+1%O_2 and 95%CO_2+5%SO_2. When injecting impurities, the chromatographic partitioning can be observed inside the gas plume and in the aqueous solution. Modeling injection of 95%CO_2+4%N_2+1%O_2 demonstrated potential usage of noble gases for monitoring and proved the previous

laboratory results. The plume composition strongly depends on a type of the co-injected gas. Moreover, a type of impurity and its concentration change the density of gas current and the density of the formation water with dissolved components. Both densities in the case of 95%CO_2+5%SO_2 injection are overall higher than those in the 95%CO_2+4%N_2+1%O_2 model. This impacts on the buoyancy forces, hence on the distance, velocity and shape of the plume. Since dissolved impurities contribute to the liquid density, it can then accelerate or slow convective dissolution. Heterogeneous gas composition induces density driven motion that can be especially important in case of heavy compounds such as SO_2.

Modeling multiphase multicomponent flow and reactive transport and accurate thermodynamic modeling of real behavior of mixtures (such as CO_2, N_2, O_2, Ar, SO_2, CH_4, H_2S, H_2O, H_2) can provide insightful understanding of coupled complex physical processes and build confidence in the sustainability of CO_2 storage sites.

References

[1] Kather, A. CO2 quality and other relevant issues. In 2nd working group meeting on CO2 quality and other relevant issues, Cottbus, Germany (2009).

[2] Ussiri, D. A., and Lal, R. Carbon Sequestration for Climate Change Mitigation and Adaptation. Springer, 2017.

[3] Bachu, S., and Bennion, D. B. Chromatographic partitioning of impurities contained in a CO2 stream injected into a deep saline aquifer: Part 1. effects of gas composition and in situ conditions. International Journal of Greenhouse Gas Control 3, 4 (2009), 458–467.

[4] Li, H., and Yan, J. Evaluating cubic equations of state for calculation of vapor–liquid equilibrium of CO2 and CO2-mixtures for CO2 capture and storage processes. Applied Energy 86, 6 (2009), 826–836.

[5] Ziabakhsh-Ganji, Z., and Kooi, H. Sensitivity of the co 2 storage capacity of underground geological structures to the presence of so 2 and other impurities. Applied Energy 135 (2014), 43–52.

[6] Ziabakhsh-Ganji, Z., and Kooi, H. An equation of state for thermodynamic equilibrium of gas mixtures and brines to allow simulation of the effects of impurities in subsurface co2 storage. International Journal of Greenhouse Gas Control 11 (2012), S21–S34.

[7] Sterpenich, J., Dubessy, J., Pironon, J., Renard, S., Caumon, M.-C., Randi, A., Jaubert, J.-N., Favre, E., Roizard, D., Parmentier, M., et al. Role of impurities on co2 injection: ex- perimental and numerical simulations of thermodynamic properties of water-salt-gas mixtures (co2+ co-injected gases) under geological storage conditions. Energy Procedia 37 (2013), 3638–3645.

[8] Corvisier, J., Bonvalot, A., Lagneau, V., Chiquet, P., Renard, S., Sterpenich, J., and Pironon, J. Impact of co-injected gases on CO2 storage sites: Geochemical modeling of experimental results. In Proceedings of the International Conference on Greenhouse Gas Technology 11, Kyoto (2013), vol. 37, Energy Procedia, pp. 3699–3710.

[9] Corvisier, J., Hajiw, M., El Ahmar, E., Coquelet, C., Sterpenich, J., Privat, R., Jaubert, J.-N., Ballerat-Busserolles, K., Coxam, J.-Y., Ce´zac, P., et al. Simulations of the impact of co-injected gases on co2 storage, the sigarrr project: processes and geochemical approaches for gas-water-salt interactions modeling. Energy Procedia 114 (2017), 3322–3334.

[10] Xu, T., Apps, J. A., Pruess, K., and Yamamoto, H. Numerical modeling of injection and mineral trapping of co2 with h2s and so2 in a sandstone formation. Chemical Geology 242, 3-4 (2007), 319–346.

[11] Xiao, Y., Xu, T., and Pruess, K. The effects of gas-fluid-rock interactions on CO2 injection and storage: Insights from reactive transport modeling. Energy Procedia 1, 1 (2009), 1783–1790.

[12] Wei, N., Li, X., Wang, Y., Wang, Y., and Kong, W. Numerical study on the field-scale aquifer storage of CO2 containing N2. Energy Procedia 37 (2013), 3952–3959.

[13] Sin, I. Numerical simulation of compressible two-phase flow and reactive transport in porous media. Applications to the study of CO2 storage and natural gas reservoirs. PhD thesis, MINES ParisTech, 2015, https://pastel.archives-ouvertes.fr/tel-01306860/document.

[14] Todaka, N., and Xu, T. Reactive transport simulation to assess geochemical impact of impurities on co2 injection into siliciclastic reservoir at the otway site, australia. International Journal of Greenhouse Gas Control 66 (2017), 177–189.

[15] Wei, N., Li, X., Wang, Y., Zhu, Q., Liu, S., Liu, N., and Su, X. Geochemical impact of aquifer storage for impure CO_2 containing O_2 and N_2: Tongliao field experiment. Applied Energy 145 (2015), 198–210.

[16] Al-Siyabi, I. Effect of impurities on CO2 stream properties. PhD thesis, Heriot-Watt University, 2013.

[17] van der Lee, J., de Windt, L., Lagneau, V., and Goblet, P. Module-oriented modeling of reactive transport with HYTEC. Computers & Geosciences 29, 3 (2003), 265–275.

[18] Lagneau, V., and van der Lee, J. Operator-splitting-based reactive transport models in strong feed- back of porosity change: The contribution of analytical solutions for accuracy validation and estimator improvement. Journal of contaminant hydrology 112, 1 (2010), 118–129.

[19] Sin, I., Lagneau, V., and Corvisier, J. Integrating a compressible multicomponent two-phase flow into an existing reactive transport simulator. Advances in Water Resources 100 (2017), 62–77.

[20] van der Lee, J. Thermodynamic and mathematical concepts of CHESS. Tech. Rep. RT-20093103- JVDL, Ecole des Mines de Paris, Centre de Geosciences, Fontainebleau, France, 2009.

[21] Corvisier, J., and Sin, I. Considering non-ideal gas mixtures in geochemical modeling of gas-water- salt-rock interactions: Application to impure co2 geological storage. GHGT-14 Melbourne-Australia (2018).

[22] Carrayrou, J., Hoffmann, J., Knabner, P., Kra¨utle, S., De Dieuleveult, C., Erhel, J., Van Der Lee, J., Lagneau, V., Mayer, K. U., and Macquarrie, K. T. Comparison of numerical methods for simulating strongly nonlinear and heterogeneous reactive transport problems — the MoMaS benchmark case. Computational Geosciences 14, 3 (2010), 483–502.

[23] Lagneau, V., and van der Lee, J. HYTEC results of the MoMaS reactive transport benchmark. Computational Geosciences 14, 3 (2010), 435–449.

[24] de Windt, L., Burnol, A., Montarnal, P., and Van Der Lee, J. Intercomparison of reactive transport models applied to UO2 oxidative dissolution and uranium migration. Journal of contaminant hydrology 61, 1 (2003), 303–312.

[25] de Windt, L., and Devillers, P. Modeling the degradation of Portland cement pastes by biogenic organic acids. Cement and Concrete Research 40 (2010), 1165–1174.

[26] Debure, M., de Windt, L., Frugier, P., and Gin, S. HLW glass dissolution in the presence of magnesium carbonate: Diffusion cell experiment and coupled modeling of diffusion and geochemical interactions. Journal of Nuclear Materials 443 (2013), 507–521.

[27] Hajiw, M., Corvisier, J., El Ahmar, E., and Coquelet, C. Impact of impurities on co 2 storage in saline aquifers: Modelling of gases solubility in water. International Journal of Greenhouse Gas Control 68 (2018), 247–255.

[28] Jacquemet, N., Pironon, J., Lagneau, V., and Saint-Marc, J. Armouring of well cement in H2S-CO2 saturated brine by calcite coating-experiments and numerical modeling. Applied Geochemistry 27 (2012), 782–795.

[29] Regnault, O., Lagneau, V., and Fiet, N. 3D reactive transport simulations of uranium in situ leaching: Forecast and process optimization. In Proceedings of the 7th International Conference on Uranium Mining and Hydrogeology, Sept 21-25 2014, Freiberg, Germany. (2014), B. Merkel and A. Arab, Eds., pp. 725–730.

[30] Hajiw, M., Chapoy, A., and Coquelet, C. Hydrocarbons–water phase equilibria using the cpa equation of state with a group contribution method. The Canadian Journal of Chemical Engineering 93, 2 (2015), 432–442.

[31] Grenthe, I., Plyasunov, A. V., and Spahiu, K. Estimations of medium effects on thermodynamic data. Modelling in aquatic chemistry 325 (1997).

[32] Robinson, D. B., and Peng, D.-Y. The characterization of the heptanes and heavier fractions for the GPA Peng-Robinson programs. Tech. rep., 1978.

[33] Jaubert, J.-N., and Mutelet, F. VLE predictions with the Peng–Robinson equation of state and temperature dependent kij calculated through a group contribution method. Fluid Phase Equilibria 224, 2 (2004), 285–304.

[34] Ahlers, J., and Gmehling, J. Development of an universal group contribution equation of state: I. Prediction of liquid densities for pure compounds with a volume translated Peng–Robinson equation of state. Fluid Phase Equilibria 191, 1 (2001), 177–188.

[35] Bachu, S., Pooladi-Darvish, M., and Hong, H. Chromatographic partitioning of impurities (H2S) contained in a CO2 stream injected into a deep saline aquifer: Part 2. effects of flow conditions. International Journal of Greenhouse Gas Control 3, 4 (2009), 468 – 473.

[36] McCain Jr., W. Reservoir-fluid property correlations-state of the art. SPE Reservoir Engineering 6, 02 (1991), 266–272.

[37] Brooks, R., and Corey, A. Hydraulic properties of porous media. Hydrology Papers, Colorado State University (1964).

[38] Ennis-King, J., Dance, T., Xu, J., Boreham, C., Freifeld, B., Jenkins, C., Paterson, L., Sharma, S., Stalker, L., and Underschultz, J. The role of heterogeneity in co2 storage in a depleted gas field: history matching of simulation models to field data for the co2crc otway project, australia. Energy Procedia 4 (2011), 3494–3501.